LETTER

A mutation–independent approach for muscular dystrophy via upregulation of a modifier gene

Dwi U. Kemaladewi[1,2,9], Prabhpreet S. Bassi[1,3,9], Steven Erwood[1,3], Dhekra Al-Basha[4,5], Kinga I. Gawlik[6], Kyle Lindsay[1], Elzbieta Hyatt[1], Rebekah Kember[1], Kara M. Place[1], Ryan M. Marks[1], Madeleine Durbeej[6], Steven A. Prescott[4,5,7], Evgueni A. Ivakine[1,10] & Ronald D. Cohn[1,3,8,10]*

Neuromuscular disorders are often caused by heterogeneous mutations in large, structurally complex genes. Targeting compensatory modifier genes could be beneficial to improve disease phenotypes. Here we report a mutation-independent strategy to upregulate the expression of a disease-modifying gene associated with congenital muscular dystrophy type 1A (MDC1A) using the CRISPR activation system in mice. MDC1A is caused by mutations in *LAMA2* that lead to nonfunctional laminin-α2, which compromises the stability of muscle fibres and the myelination of peripheral nerves. Transgenic overexpression of *Lama1*, which encodes a structurally similar protein called laminin-α1, ameliorates muscle wasting and paralysis in mouse models of MDC1A, demonstrating its importance as a compensatory modifier of the disease[1]. However, postnatal upregulation of *Lama1* is hampered by its large size, which exceeds the packaging capacity of vehicles that are clinically relevant for gene therapy. We modulate expression of *Lama1* in the *dy^{2j}/dy^{2j}* mouse model of MDC1A using an adeno-associated virus (AAV9) carrying a catalytically inactive Cas9 (dCas9), VP64 transactivators and single-guide RNAs that target the *Lama1* promoter. When pre-symptomatic mice were treated, *Lama1* was upregulated in skeletal muscles and peripheral nerves, which prevented muscle fibrosis and paralysis. However, for many disorders it is important to investigate the therapeutic window and reversibility of symptoms. In muscular dystrophies, it has been hypothesized that fibrotic changes in skeletal muscle are irreversible. However, we show that dystrophic features and disease progression were improved and reversed when the treatment was initiated in symptomatic *dy^{2j}/dy^{2j}* mice with apparent hindlimb paralysis and muscle fibrosis. Collectively, our data demonstrate the feasibility and therapeutic benefit of CRISPR–dCas9-mediated upregulation of *Lama1*, which may enable mutation-independent treatment for all patients with MDC1A. This approach has a broad applicability to a variety of disease-modifying genes and could serve as a therapeutic strategy for many inherited and acquired diseases.

MDC1A is caused by mutations in the *LAMA2* gene—which encodes laminin-α2 chain. LAMA2 polymerizes with the β1 and γ1 chains to form the heterotrimer laminin-211, which is an extracellular matrix protein complex. Interactions between laminin-211, α-dystroglycan and α7β1 integrin in skeletal muscles and Schwann cells is important for the survival and stability of myotubes, proper neurite growth, axon myelination and migration of Schwann cells. Lack of laminin-211 in MDC1A causes degeneration of skeletal muscle and impaired differentiation of Schwann cells, resulting in a cascade of secondary events that include apoptosis or necrosis of muscle fibres, inflammation and fibrosis, which ultimately precipitate the disease. Despite considerable advances in our understanding of the pathophysiology that underlies MDC1A, there is currently no cure.

Owing to the genetic nature of the disease, the correction of *LAMA2* mutations is a promising treatment option for MDC1A. We recently described the use of CRISPR–Cas9 technology to correct a mutation in *Lama2* in vivo[2]. We focused on the *dy^{2j}/dy^{2j}* mouse model; *dy^{2j}/dy^{2j}* mice have a splice site mutation in *Lama2* that causes spontaneous exon skipping and truncation of the N-terminal domain of the protein[3]. We developed an exon-inclusion strategy to correct the splice site mutation, leading to restoration of full-length Lama2, which established the direct correction of the primary genetic defect that underlies MDC1A in an in vivo model[2]. Nevertheless, there are over 350 pathogenic nonsense, missense, splice site and deletion mutations in *LAMA2* reported to date. Given the number of MDC1A-causing genomic alterations, CRISPR–Cas9-mediated correction would require the design and thorough analysis of multiple single-guide RNAs (sgRNAs) that are specific to each mutation. Moreover, safety concerns regarding the potential mutagenic nature of the CRISPR–Cas9 system and the presence of off-target effects after gene editing remain, which together may prove to be challenging from a safety and regulatory point-of-view.

By contrast, the attenuation of disease pathogenicity by targeted modulation of the expression of disease-modifier genes would be a potentially safer alternative and beneficial to all individuals with MDC1A. One of the strongest reported disease modifiers for MDC1A is laminin-α1, which is structurally similar to laminin-α2 (Fig. 1a). However, laminin-α1 is not expressed in skeletal muscles or Schwann cells. Previous studies have demonstrated that transgenic *Lama1* overexpression rescued myopathy and peripheral neuropathy in *dy^{2j}/dy^{2j}* mice[4] and *dy^{3K}/dy^{3K}* mice[1,4,5]; the latter also had an increased lifespan. Although these studies established a compensatory function of laminin-α1 in MDC1A, the use of this modifier as postnatal gene therapy is hampered by the size of the *Lama1* cDNA, which exceeds the packaging capacity of AAV vectors.

Advances in CRISPR–Cas9 technologies have provided opportunities for regulating gene expression and creating epigenetic alterations without introducing DNA double-stranded breaks, which are known as the CRISPR transcriptional activation system. The strategy uses nuclease-deficient Cas9 (dCas9), which is unable to cleave DNA owing to mutations within the nuclease domains and retains the ability to specifically bind to DNA when guided by a sgRNA[6,7]. Using the previously described *Streptococcus pyogenes* (*Sp*)dCas9 fused to multiple copies of the VP16 transcriptional activator, our group and others have demonstrated the use of the CRISPR–dCas9 system to upregulate expression of modifier genes in vitro[6–8]. A major challenge for in vivo applications lies in the large size of *Sp*dCas9 and its transcriptional activator fusion derivatives that exceed the genome-packaging capacity of AAVs.

[1]Program in Genetics and Genome Biology, the Hospital for Sick Children Research Institute, Toronto, Ontario, Canada. [2]Department of Pediatrics, University of Pittsburgh School of Medicine, Pittsburgh, PA, USA. [3]Department of Molecular Genetics, University of Toronto, Toronto, Ontario, Canada. [4]Program in Neurosciences and Mental Health, the Hospital for Sick Children Research Institute, Toronto, Ontario, Canada. [5]Department of Physiology, University of Toronto, Toronto, Ontario, Canada. [6]Unit of Muscle Biology, Department of Experimental Medical Science, Lund University, Lund, Sweden. [7]Institute of Biomaterials and Biomedical Engineering, University of Toronto, Toronto, Ontario, Canada. [8]Department of Pediatrics, the Hospital for Sick Children, Toronto, Ontario, Canada. [9]These authors contributed equally: Dwi U. Kemaladewi, Prabhpreet S. Bassi. [10]These authors jointly supervised this work: Evgueni A. Ivakine, Ronald D. Cohn. *e-mail: ronald.cohn@sickkids.ca
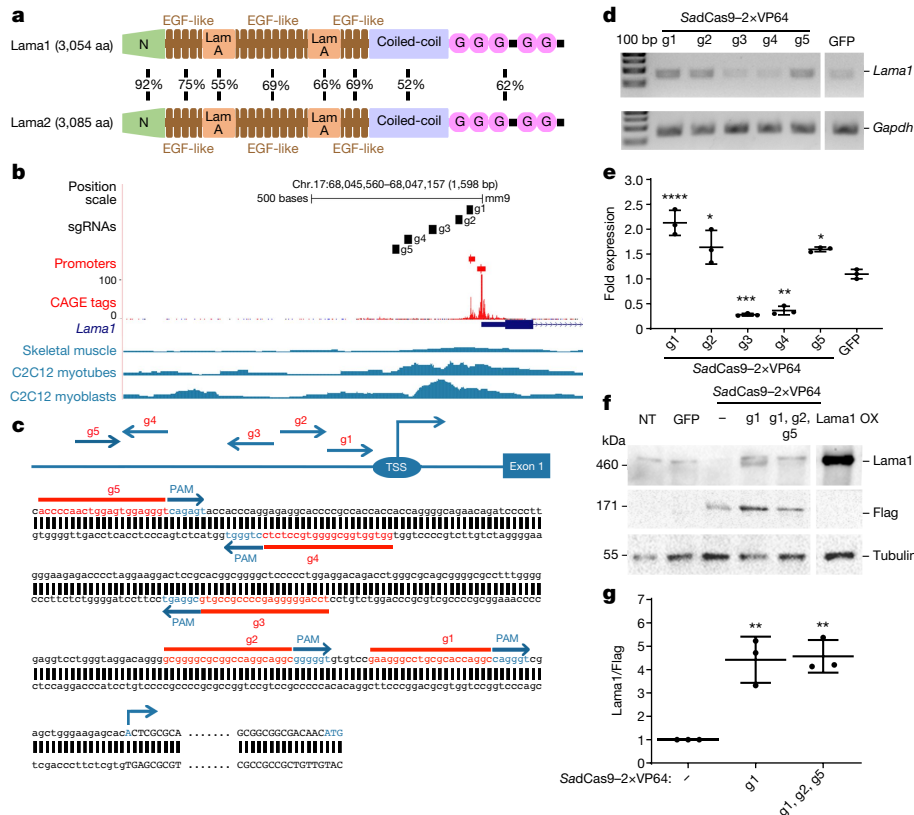
Fig. 1 | SadCas9–2×VP64-mediated upregulation of *Lama1* in vitro.
a, Protein alignment of Lama1 and Lama2. The total number of amino acids (aa) and percentage similarity between each domain are indicated. EGF, epidermal growth factor; G, globular; N, N terminus. **b**, Analyses of the proximal promoter of *Lama1*. Five sgRNAs (g1–g5) were designed to target the proximal promoter region of *Lama1* immediately upstream of the transcription start site, as indicated by CAGE tags (red). Chromatin accessibility in skeletal muscle tissue and cells (retrieved using Digital DNase footprinting and assay for transposase-accessible chromatin using sequencing (ATAC-seq)) are shown in blue. Data were plotted according to positions from the UCSC Genome Browser. **c**, Positions of the five sgRNAs relative to *Lama1* transcription start site. Arrowheads indicate the direction of each sgRNA. Sequences of each sgRNA (red) are immediately downstream (5′) of *Sa* protospacer adjacent motif (PAM) sequences (NNGRRT) (in blue). TSS, transcription start site. Lowercase and uppercase letters indicate intronic and exonic sequences, respectively. ATG indicates the translation start site. **d**, **e**, C2C12 myoblasts were transfected with a plasmid encoding SadCas9–2×VP64 and the corresponding sgRNA(s) targeting *Lama1* and, 72 h after transfection, were analysed by reverse transcription PCR (RT–PCR) (**d**) and quantitative reverse transcription PCR (qRT–PCR) (**e**). **d**, A 100-bp ladder is shown. **e**, Data are mean ± s.d. from $n = 3$ biologically independent samples. *P* values are (from left to right): ****$P < 0.0001$, *$P = 0.0136$, ***$P = 0.0006$, **$P = 0.0015$, *$P = 0.0224$; one-way ANOVA. Basal *Lama1* expression in GFP-transfected cells was set to 1. **f**, **g**, Single and a combination of the optimal sgRNAs were transfected into dy^{2j}/dy^{2j} myoblasts and expression of Lama1 was assessed by western blot (**f**); quantification is shown as fold change in expression (**g**). Flag expression serves as a transfection control and is used to normalize the Lama1 upregulation. NT, not transfected. '−', no sgRNA. **g**, Data are mean ± s.d. from $n = 3$ biologically independent samples. *P* values are compared to 'no sgRNA': **$P = 0.0023$ (middle), **$P = 0.0019$ (right); one-way ANOVA. **d–g**, Experiments were repeated three times independently with similar results.

To accommodate this limitation, we adapted the transcriptional upregulation system and used a considerably smaller Cas9 protein, which is derived from *Staphylococcus aureus* (*Sa*)[9], to upregulate Lama1. We hypothesized that CRISPR–dCas9-mediated transcriptional upregulation of *Lama1* would be sufficient to compensate for the lack of *Lama2* and ameliorate disease phenotypes in dy^{2j}/dy^{2j} mice.

First, we mutagenized the endonuclease catalytic residues (D10A, N580A) of *Sa*Cas9 to create *Sa*dCas9 and then fused it to transcriptional activators VP64 (four copies of VP16) on both N and C termini (Extended Data Fig. 1). We tested the ability of the system (hereafter SadCas9–2×VP64) to upregulate the expression of a minCMV-driven tdTomato gene in HEK293T cells. In the presence of SadCas9–2×VP64 and an sgRNA that targets the minCMV locus, we observed a high tdTomato fluorescence signal, which indicates the general applicability of this system to modulate expression of a gene of interest.

Subsequently, we tailored the system to upregulate *Lama1* expression and designed five sgRNAs, denoted as g1 to g5, within the 500-nucleotide region immediately upstream of the *Lama1* transcription start site (Fig. 1b, c). When co-expressed with SadCas9–2×VP64, three out of five sgRNAs (namely g1, g2 and g5) consistently induced a significant increase in *Lama1* transcript expression in C2C12 mouse myoblasts (Fig. 1d, e), as well as protein expression in dy^{2j}/dy^{2j}-derived myoblasts (Fig. 1f, g), warranting further investigation in vivo.

We then treated three-week-old dy^{2j}/dy^{2j} mice with an AAV9 that contained Flag-tagged SadCas9–2×VP64 in the absence of sgRNA (no guide) or with g1 (single guide) or a combination of g1, g2 and g5 (three guides) (Fig. 2a). Owing to the packaging capacity of the AAV, dCas9–2×VP64 and the three guides were split into two vectors (Fig. 2a). Each mouse received a single intramuscular injection of 7.5×10^{11} viral genomes of AAV9—which was doubled to 1.5×10^{12} viral genomes in total for the three-guide cohort—in the right tibialis anterior muscle, and was euthanized 4 weeks after injection. Flag expression was detected by western blot in all SadCas9–2×VP64-injected right tibialis anterior muscles; however, only those injected with guide-containing constructs showed upregulation of Lama1 (Fig. 2b). Similarly, immunofluorescence staining revealed the expression of Lama1 in the sarcolemma (Fig. 2c), indicating proper protein localization. Analysis of haematoxylin and eosin staining showed that mice in the single- and three-guide treatment groups had considerably improved muscle architecture (Fig. 2c), compared to the no-guide controls.
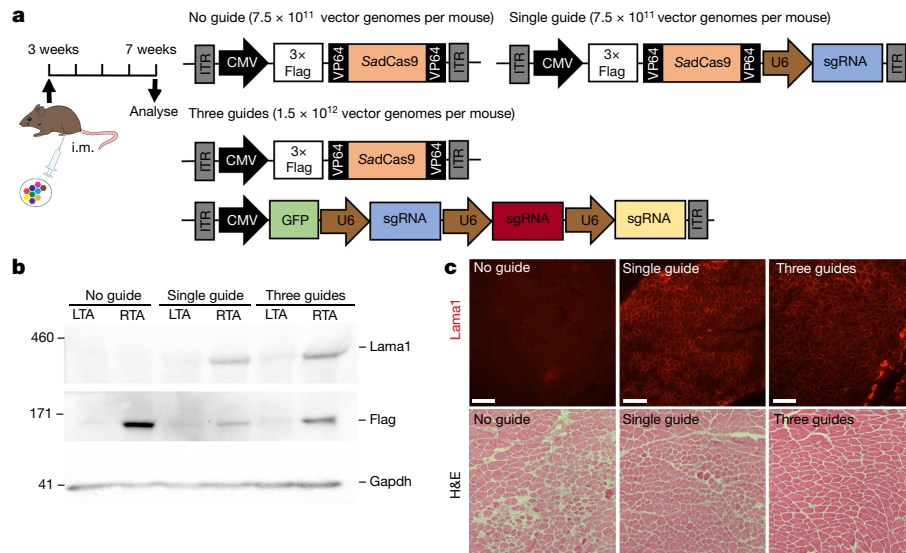
Fig. 2 | Upregulation of Lama1 in tibialis anterior muscles of dy^{2j}/dy^{2j} mice improves muscle fibrosis. a, Right tibialis anterior muscles of three-week-old dy^{2j}/dy^{2j} mice were injected with AAV9s containing no guide ($n = 4$; 7.5×10^{11} viral genomes), a single guide ($n = 4$; 7.5×10^{11} viral genomes) or three guides ($n = 4$; split into two vectors; total dose of $2 \times 7.5 \times 10^{11}$ viral genomes). i.m., intramuscular; ITR, inverted terminal repeats. CMV and U6 promoters are depicted as arrows. Left tibialis anterior muscles serve as control. **b**, Western blot analysis of Lama1, Flag-tagged SadCas9 and Gapdh expression. LTA, left tibialis anterior muscle; RTA, right tibialis anterior muscle. **c**, Immunofluorescence images of Lama1 (top) and haematoxylin and eosin (H&E) (top) of cross-sections of right tibialis anterior muscles from each treatment group. Scale bars, 50 μm. Samples from all mice ($n = 4$ mice per group) were analysed twice independently with similar results.

Next, we investigated whether upregulation of *Lama1* could be achieved systemically in vivo and, if administered in presymptomatic neonatal dy^{2j}/dy^{2j} mice, whether it would prevent the manifestation of dystrophic pathophysiology and paralysis (Extended Data Fig. 2). AAV9 particles that contained either no guide or a combination of three guides were injected into the temporal vein of two-day-old (P2) dy^{2j}/dy^{2j} mice (Extended Data Fig. 2a). Then, seven weeks after injection, Lama1 expression was detected in the tibialis anterior (Extended Data Fig. 2b) and gastrocnemius (Extended Data Fig. 2c) muscles. Although AAV transduction efficiency varied slightly between individual muscles, overall upregulation of Lama1 led to a reduction in fibrosis (Extended Data Fig. 2d–h), larger fibre size (Extended Data Fig. 2g, i), as well as an absence of classical hindlimb contracture (Supplementary Videos 1, 2). Collectively, these data show successful prevention of the disease pathophysiology upon early intervention in dy^{2j}/dy^{2j} mice.

We subsequently examined the ability of *Lama1* upregulation to reverse established muscular and peripheral nerve dysfunction by initiating the treatment at three weeks of age, when paralysis was already apparent[10] (Fig. 3a). We first tested three different doses that ranged from 7.5×10^{10} to 3×10^{11} viral genomes per gram of mouse per AAV9, which was doubled for the three-guide cohorts owing to the use of two vectors, and found that the highest dose resulted in homogeneous Lama1-positive fibres (Extended Data Fig. 3a) and significant improvement of muscle function and mobility (Extended Data Fig. 3b, c). Longitudinal measurements of mouse mobility and stand-up activity in a non-invasive open field activity assay showed a significant difference between the no-guide- and three-guide-treated mice starting at five and six weeks old, respectively, which was sustained over time (Fig. 3b, c). Furthermore, specific tetanic force, which measures the aggregate torque produced by the dorsiflexor muscles, was also improved in the three-guide-treated mice (Fig. 3d). Consistent with this finding, we observed a significant increase in nerve conduction velocity, which is indicative of restoration of the myelination defect and contributes to neuromuscular functionality (Fig. 3e). The absence of paralysis in the hindlimbs and markedly improved movement of the mice were evident at the end of the treatment regimen (Supplementary Videos 3, 4).

Molecular analysis of the treated mice revealed strong expression of Lama1 by immunostaining and western blot (Fig. 3f, g and Extended Data Fig. 4), which was accompanied by normalization of the expression of the α4 chain of the laminin subunit[4] (Extended Data Figs. 5, 6), significant improvement in muscle histopathology (Fig. 3h) and approximately 50% reduction in the fibrotic area (Fig. 3i) compared to the no-guide control group. There was a trend towards larger fibres in the treated mice, although it did not reach statistical significance owing to the large variation between mice (Fig. 3j). In addition, upregulation of Lama1 was also observed in the endoneurium of sciatic nerves and resulted in restoration of the myelination defect (Fig. 3k and Extended Data Fig. 7), supporting the improvement of nerve conduction velocity and lack of paralysis in the mice (Fig. 3e and Supplementary Videos 3, 4). Quantification of the AAV genome copy number revealed accumulation of most of the viral genomes in the liver, which is expected from intravenous delivery. Nevertheless, approximately 1.11 ± 0.4 (mean $\pm$ s.e.m.) and 34.1 ± 4.3 copies per diploid genome of the viral genome were detected in the sciatic nerves and skeletal muscles, respectively (Extended Data Fig. 8). Even the relatively low transduction efficiency in sciatic nerves—compared to other tissues such as the skeletal muscle and liver—was sufficient to induce functionally significant expression of Lama1.

Finally, we investigated the genome-wide effects of CRISPR–dCas9-mediated upregulation of Lama1 by performing RNA sequencing on quadriceps muscles (Extended Data Figs. 9, 10 and Supplementary Tables 1–3). We observed a 3.6-fold upregulation (log_2-transformed value) of Lama1 (defined by false-discovery rate-adjusted $P < 0.05$) when comparing the mice treated with AAV9 that contained no guide and three guides (Extended Data Fig. 9a). The transcriptional change was even higher (log_2-transformed change in expression of 9-fold) when comparing untreated dy^{2j}/dy^{2j} with three-guide-treated dy^{2j}/dy^{2j} mice (Extended Data Fig. 9b, c). Hierarchical clustering between groups revealed clustering between wild-type mice and three-guide-treated mice, whereas the untreated cohort was grouped together with no-guide-treated mice (Extended Data Figs. 9d, 10). We also computationally predicted 704 potential off-target binding sites for the three sgRNAs that target the *Lama1* promoter in the mouse genome, selected based on the presence of a six-base-pair (bp) proximal seed sequence of the protospacer adjacent motif and fewer than ten total mismatches to the cognate target sequence (Supplementary
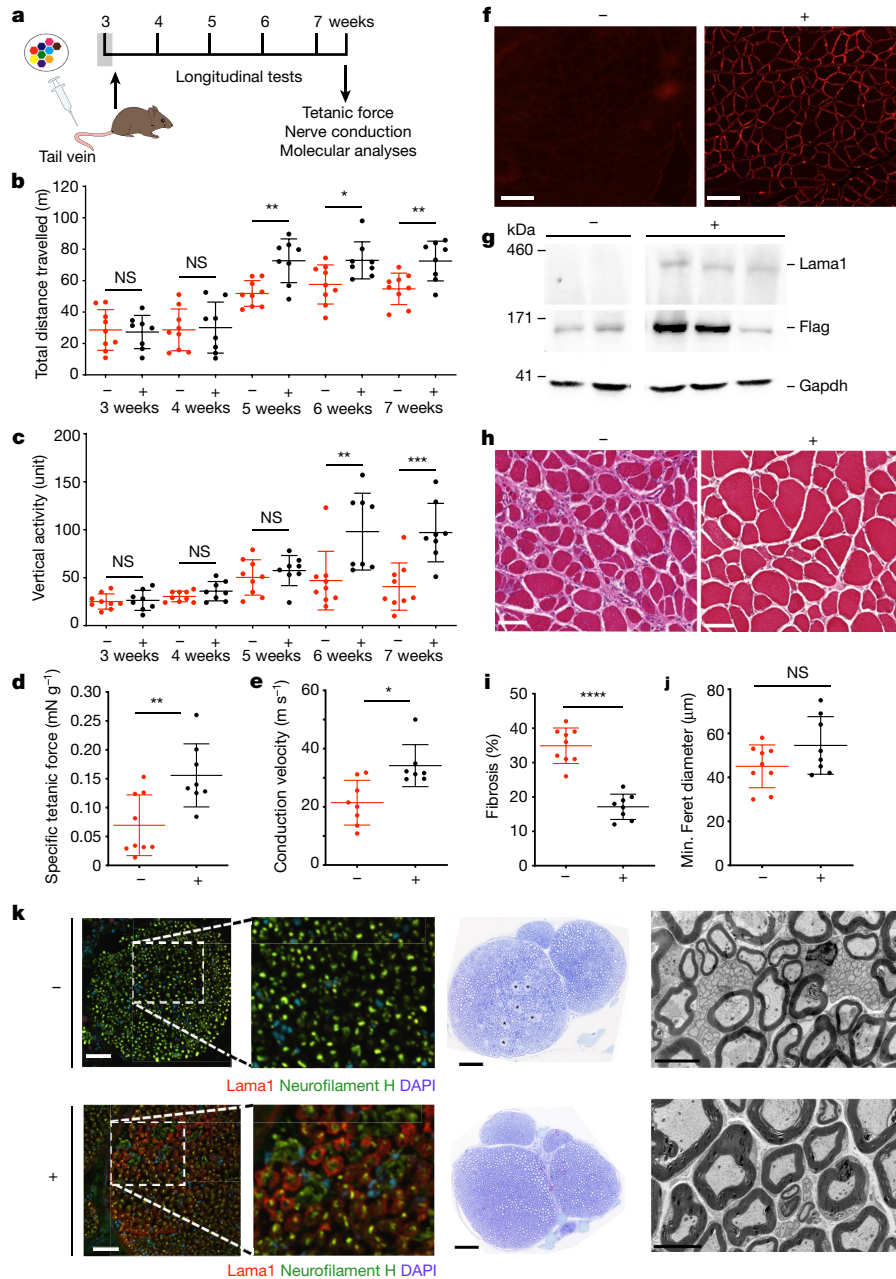
Fig. 3 | Upregulation of Lama1 in older dy^{2j}/dy^{2j} mice halts disease progression. a, Three-week-old dy^{2j}/dy^{2j} mice were injected with AAV9s containing no guide (denoted as '−'; $n = 9$; 3×10^{11} viral genomes g^{-1} of mouse) or three guides (denoted as '+'; $n = 8$; split into two vectors; total dose of $2 \times 3 \times 10^{11}$ viral genomes g^{-1} of mouse) in the tail vein. Grey box represents the period before treatment. **b**, **c**, The open field activity assay was performed weekly, before (indicated as 3 weeks) and after treatment. NS, not significant. **d**, **e**, The mice were tested for muscle contractile properties (**d**) and nerve conduction velocity (**e**) at the end of the treatment regimen. **b–e**, Data are mean ± s.d.; two-tailed t-test. **b**, P values from left to right (including NS) are: $P = 0.8230$, $P = 0.8467$, **$P = 0.0017$, *$P = 0.0201$, *$P = 0.0056$. **c**, P values from left to right (including NS) are: $P = 0.8026$, $P = 0.1725$, $P = 0.4061$, **$P = 0.0094$, *$P = 0.0008$. **d**, **$P = 0.0047$. **e**, **$P = 0.0059$. Note that the number of mice analysed in the experiment shown in **e** were $n = 8$ (no guide) and $n = 7$ (three guides). **f**, **g**, Immunofluorescence (**f**) and western blot (**g**)

analyses were carried out to analyse Lama1 expression. **h–j**, Haematoxylin and eosin staining (**h**) to quantify fibrosis (**i**; ****$P < 0.0001$, two-tailed t-test) and fibre size (**j**; $P = 0.117$, two-tailed t-test) was performed on gastrocnemius muscles. All mice ($n = 9$, no guide; $n = 8$, three guides) were analysed for experiments in **f–j**, which were repeated three times independently with similar results. **k**, Left, sciatic nerves were stained for expression of Lama1 (red) and neurofilament H (green). Nuclei were counterstained using 4′,6-diamidino-2-phenylindole (DAPI) (blue). Higher-magnification images from the dotted area are shown to the right. Middle, representative toluidine blue images are shown for each group. Asterisks indicate a region of amyelinated axon fibres. Right, electron micrographs are shown for each group. Three mice per group were analysed for the experiment in **k**, which was repeated three times independently with similar results. Scale bars, 100 μm (**f**), 50 μm (**h**) and 200 μm (**k**).

Tables 4, 5). None of the top 100 genes contained a predicted off-target site within 60 kilobases of the gene body and the mean distance from off-target site to the gene body was 2.2 megabases.

Taken together, our results provide strong evidence of the robustness and durability of CRISPR–dCas9-mediated upregulation of Lama1 for

the treatment of MDC1A. Additionally, we show the therapeutic promise of the strategy for reversal of dystrophic features in skeletal muscle and peripheral neuropathy in the dy^{2j}/dy^{2j} mouse model of MDC1A, which ultimately halts progression of the disease, without any confounding off-target effects.

One challenge in developing a therapy for the treatment of MDC1A is that the heterogeneity of mutations often leads to variable disease severity and progression. Therefore, there is an urgent need to develop a universal, mutation-independent strategy that provides a treatment approach for all patients with MDC1A. Our study establishes a framework in which transcriptional upregulation of a disease-modifier gene, such as *Lama1*, ameliorates disease symptoms in vivo and has the potential to be applied to all patients with MDC1A, irrespective of the causative mutation. The ability to modify gene expression in postnatal mice also allowed us to begin to investigate the therapeutic window of intervention and address an important question in the development of therapeutics and clinical trials for the treatment of MDC1A[11], such as the reversibility of symptoms caused by muscle fibrosis and nerve abnormalities. Here we show that upregulation of *Lama1* leads to significant rescue of the phenotypes in three-week-old mice with already-apparent muscle fibrosis and hindlimb paralysis, indicating that postsymptomatic treatment provides a considerable benefit in the dy^{2j}/dy^{2j} mouse model.

Previous studies have demonstrated that the peripheral neuropathy found in the dy^{2j}/dy^{2j} mice involves impaired radial sorting, which originates prenatally owing to a lack of *Lama2* in (immature) Schwann cells that prevents the cells from proliferating and differentiating properly. Many therapeutic interventions that start during the perinatal period (for example, at P2) influence the proliferation and differentiation of Schwann cells[12,13]. As our intervention starts at three weeks of age, it is unlikely that our strategy affects the proliferation and differentiation of Schwann cells and their progenitors. Nevertheless, the radial sorting process is not completely abolished in adult dy^{2j}/dy^{2j} Schwann cells[14]. In fact, dy^{2j}/dy^{2j} Schwann cells at P28 retain a limited capacity to initiate radial sorting that leads to partially impaired postnatal myelination, in which cooperation between Lama2 and its receptors—such as dystroglycan, α6β1 and α6β4 integrins—is crucial[15]. Therefore, we suggest that *Lama1* upregulation compensated for the lack of *Lama2* by establishing interactions with the integrins and/or dystroglycan in the basal lamina, which eventually restored the myelination defect. Examination of Lama1 interactomes would be required to investigate the cellular mechanism of the compensatory effect of postnatal *Lama1* upregulation. Furthermore, previous studies[14,15] have reported differences in the radial sorting defect between roots and proximal nerves of dy^{2j}/dy^{2j} mice, compared to their distal nerves. Additional studies to explore the effect of postnatal *Lama1* upregulation on spatial differences in axonal radial sorting would be important both from disease mechanistic and translational perspectives.

In addition to Lama1, a number of disease-modifying strategies are currently being explored in animal models of MDC1A, including miniaturized agrin (mini agrin)[13,16], laminin-α1 LN-domain nidogen-1 (αLNNd) and a combination of both[17,18]. Although the efficacy of αLNNd and the combination of αLNNd and mini agrin have only been explored in transgenic mice thus far[17], AAV-mediated delivery of mini agrin has been shown to normalize most histopathological parameters in skeletal muscle, and improve myelination and regeneration of Schwann cells of the peripheral nerves in the more severe dy^W/dy^W mouse model[13]. Despite the observed phenotypic improvements, the mini-agrin-treated dy^W/dy^W mice still have a lower survival rate than wild-type mice that expressed full-length agrin, suggesting a potential limitation of the strategy. It is important to note that many preclinical studies of MDC1A were carried out in the more-severe dy^W/dy^W and dy^{3K}/dy^{3K} mouse models. Therefore, it will be paramount to evaluate our approach in these more-severe mouse models to assess critical parameters such as survival, which is not possible in the dy^{2j}/dy^{2j} mice, as these mice have a near-normal lifespan.

Neuromuscular disorders have provided excellent examples to demonstrate the role of disease modifiers. In addition to MDC1A, several studies have demonstrated that upregulation of *Lama1* stabilizes the sarcolemmal membrane in Duchenne muscular dystrophy. The most advanced approach is delivery of laminin-111 protein in dystrophin-deficient mice, although the need to produce a large amount of bioactive protein is challenging[19]. In addition, the use of the CRISPR–dCas9 system to upregulate Lama1 in dystrophin-deficient mice has been achieved locally using electroporation, which is not easily translatable into clinical settings[20]. Our strategy of using AAV-mediated infection of *Sa*dCas9 to upregulate *Lama1* in vivo may be tested further as a potential therapy in Duchenne muscular dystrophy. Moreover, the CRISPR–dCas9-mediated transcriptional modulation may be used in conjunction with a mutation-correction approach for which the level of restoration of the defective gene is suboptimal, therefore necessitating further amplification to reach therapeutic efficacy[2,21–23].

A recent study has described the use of the CRISPR transcriptional activation system to induce expression of target genes in skeletal muscle, kidney and liver tissues, resulting in phenotypic augmentation such as enhanced muscle mass and substantial improvement in disease pathophysiology[24]. However, it relied almost exclusively on a Cas9-expressing transgenic mouse model or on local intramuscular treatments and it is therefore difficult to extrapolate the efficacy of this strategy to disease-relevant models. By contrast, we successfully demonstrated robust upregulation of Lama1 after systemic delivery of therapeutic components in a relevant mouse model of disease that does not constitutively express Cas9.

Finally, the modular nature of the CRISPR–dCas9 system can be used not only to upregulate, but also to downregulate the expression of a target gene when coupled with the transcriptional repressor Kruppel-associated box (KRAB)[25]. An application as a combinatorial therapeutic approach, involving concurrent upregulation of protective disease-modifier genes and downregulation of detrimental genes, would represent a new paradigm for lessening disease phenotypes. In summary, our study establishes a framework to use CRISPR–dCas9 to modulate gene expression of disease modifiers that should be considered as a mutation-independent therapeutic strategy not only to treat MDC1A, but also for the treatment of various other inherited and acquired diseases.

Online content

1. Gawlik, K., Miyagoe-Suzuki, Y., Ekblom, P., Takeda, S. & Durbeej, M. Laminin α1 chain reduces muscular dystrophy in laminin α2 chain deficient mice. *Hum. Mol. Genet.* **13**, 1775–1784 (2004).
2. Kemaladewi, D. U. et al. Correction of a splicing defect in a mouse model of congenital muscular dystrophy type 1A using a homology-directed-repair-independent mechanism. *Nat. Med.* **23**, 984–989 (2017).
3. Sunada, Y., Bernier, S. M., Utani, A., Yamada, Y. & Campbell, K. P. Identification of a novel mutant transcript of laminin α2 chain gene responsible for muscular dystrophy and dysmyelination in dy^{2j} mice. *Hum. Mol. Genet.* **4**, 1055–1061 (1995).
4. Gawlik, K. I., Harandi, V. M., Cheong, R. Y., Petersén, Å. & Durbeej, M. Laminin α1 reduces muscular dystrophy in dy^{2j} mice. *Matrix Biol.* **70**, 36–49 (2018).
5. Gawlik, K. I., Li, J. Y., Petersén, A. & Durbeej, M. Laminin α1 chain improves laminin α2 chain deficient peripheral neuropathy. *Hum. Mol. Genet.* **15**, 2690–2700 (2006).
6. Maeder, M. L. et al. CRISPR RNA-guided activation of endogenous human genes. *Nat. Methods* **10**, 977–979 (2013).
7. Perez-Pinera, P. et al. RNA-guided gene activation by CRISPR–Cas9-based transcription factors. *Nat. Methods* **10**, 973–976 (2013).
8. Wojtal, D. et al. Spell checking nature: versatility of CRISPR/Cas9 for developing treatments for inherited disorders. *Am. J. Hum. Genet.* **98**, 90–101 (2016).
9. Ran, F. A. et al. In vivo genome editing using *Staphylococcus aureus* Cas9. *Nature* **520**, 186–191 (2015).
10. Kemaladewi, D. U., Benjamin, J. S., Hyatt, E., Ivakine, E. A. & Cohn, R. D. Increased polyamines as protective disease modifiers in congenital muscular dystrophy. *Hum. Mol. Genet.* **27**, 1905–1912 (2018).
11. Bönnemann, C. G. et al. Diagnostic approach to the congenital muscular dystrophies. *Neuromuscul. Disord.* **24**, 289–311 (2014).
12. Homma, S., Beermann, M. L. & Miller, J. B. Peripheral nerve pathology, including aberrant Schwann cell differentiation, is ameliorated by doxycycline in a laminin-α2-deficient mouse model of congenital muscular dystrophy. *Hum. Mol. Genet.* **20**, 2662–2672 (2011).

13. Qiao, C. et al. Amelioration of muscle and nerve pathology in LAMA2 muscular dystrophy by AAV9-mini-agrin. *Mol. Ther. Methods Clin. Dev.* **9**, 47–56 (2018).
14. Patton, B. L., Wang, B., Tarumi, Y. S., Seburn, K. L. & Burgess, R. W. A single point mutation in the LN domain of LAMA2 causes muscular dystrophy and peripheral amyelination. *J. Cell Sci.* **121**, 1593–1604 (2008).
15. Previtali, S. C. et al. Expression of laminin receptors in Schwann cell differentiation: evidence for distinct roles. *J. Neurosci.* **23**, 5520–5530 (2003).
16. Bentzinger, C. F., Barzaghi, P., Lin, S. & Ruegg, M. A. Overexpression of mini-agrin in skeletal muscle increases muscle integrity and regenerative capacity in laminin-α2-deficient mice. *FASEB J.* **19**, 934–942 (2005).
17. Reinhard, J. R. et al. Linker proteins restore basement membrane and correct *LAMA2*-related muscular dystrophy in mice. *Sci. Transl. Med.* **9**, eaal4649 (2017).
18. McKee, K. K. et al. Chimeric protein repair of laminin polymerization ameliorates muscular dystrophy phenotype. *J. Clin. Invest.* **127**, 1075–1089 (2017).
19. Rooney, J. E., Gurpur, P. B. & Burkin, D. J. Laminin-111 protein therapy prevents muscle disease in the *mdx* mouse model for Duchenne muscular dystrophy. *Proc. Natl Acad. Sci. USA* **106**, 7991–7996 (2009).
20. Perrin, A., Rousseau, J. & Tremblay, J. P. Increased expression of laminin subunit alpha 1 chain by dCas9–VP160. *Mol. Ther. Nucleic Acids* **6**, 68–79 (2017).
21. Yuan, J. et al. Genetic modulation of RNA splicing with a CRISPR-guided cytidine deaminase. *Mol Cell* **72**, 380–394 (2018).
22. Villiger, L. et al. Treatment of a metabolic liver disease by in vivo genome base editing in adult mice. *Nat. Med.* **24**, 1519–1525 (2018).
23. Bengtsson, N. E. et al. Muscle-specific CRISPR/Cas9 dystrophin gene editing ameliorates pathophysiology in a mouse model for Duchenne muscular dystrophy. *Nat. Commun.* **8**, 14454 (2017).
24. Liao, H. K. et al. *In vivo* target gene activation via CRISPR/Cas9-mediated *trans*-epigenetic modulation. *Cell* **171**, 1495–1507 (2017).
25. Thakore, P. I. et al. Highly specific epigenome editing by CRISPR–Cas9 repressors for silencing of distal regulatory elements. *Nat. Methods* **12**, 1143–1149 (2015).

Author contributions D.U.K., E.A.I. and R.D.C. conceived and supervised the study. P.S.B., K.L., R.K. and K.M.P. cloned and screened guides in vitro. D.U.K., P.S.B., K.L. and E.H. performed in vivo injections and contractile assays. D.U.K., P.S.B., K.L., K.M.P. and R.M.M. analysed muscle histology. K.I.G. and M.D. performed extended muscle imaging and provided reagents. D.U.K. performed longitudinal open field assay and vector genome quantification. D.U.K. and P.S.B. performed nerve imaging with the help from K.M.P. and R.M.M. D.U.K. and D.A.-B. performed nerve conduction velocity under supervision by S.A.P. S.E. analysed RNA-sequencing data and off-target prediction. D.U.K. wrote the manuscript with inputs from the other authors. All authors provided feedback and agreed on the final manuscript.

Competing interests The authors declare no competing interests.

Additional information
Extended data is available for this paper at https://doi.org/10.1038/s41586-019-1430-x.
Supplementary information is available for this paper at https://doi.org/10.1038/s41586-019-1430-x.
Reprints and permissions information is available at http://www.nature.com/reprints.
Correspondence and requests for materials should be addressed to R.D.C.
Publisher's note: Springer Nature remains neutral with regard to jurisdictional claims in published maps and institutional affiliations.

METHODS

Engineering of activation constructs. A fragment containing a catalytically inactive *Sa*dCas9 coupled to two flanking VP64 transactivator domains was synthesized by BioBasic Canada and cloned into pX601 (Addgene 61591) using AgeI and EcoRI directional cloning to generate 3×Flag-VP64-*Sa*dCas9(D10A/N580A)-NLS-VP64 plasmid (Fig. 2a and Supplementary Table 6). Each sgRNA (Supplementary Table 6) was subsequently introduced using BsaI directional cloning. To generate the three-guides-only construct (Fig. 2a), a fragment containing three repetitive regions of the U6 promoter and *S. aureus* guide scaffold was assembled, with short linkers in between each region (BioBasic Canada). The fragment was cloned into KpnI and NotI sites of a pX601-derivative plasmid.

Cell culture. Primary myoblasts were isolated from the extensor digitorum longus muscle of dy^{2J}/dy^{2J} mice and maintained in DMEM supplemented with 1% chicken embryo extract (GeminiBioscience), 10% horse serum, 1% penicillin–streptomycin and 1% L-glutamine (Gibco). HEK293 and C2C12 cells (ATCC) were maintained in DMEM supplemented with 10% FBS, 1% penicillin–streptomycin and 1% L-glutamine (Gibco). All cells were maintained at 37 °C with 5% CO_2.

Transfection of HEK293 cells was performed using Lipofectamine 2000. C2C12 and dy^{2J}/dy^{2J} cells were transfected in 12-well-plates using the Neon Transfection System (Invitrogen). In brief, 400,000 cells were electroporated with 1.5 μg of DNA using optimization program 16 (pulse voltage, 1,400 V; pulse width, 20 ms; pulse number, 2). Cells were grown for 72 h, after which RNA or protein was subsequently collected for protein analysis and guide screening.

Mice, virus production and injections. dy^{2J}/dy^{2J} mice were purchased from the Jackson Laboratory and maintained in The Center for Phenogenomics. Both male and female mice were used in the analyses. The numbers of mice were based on the TREAT-NMD standard operating protocol for MDC1A or a previous study[2]. All mouse experiments were performed according to Animal Use Protocol number 20-0305 (The Center for Phenogenomics). *Sa*dCas9–2×VP64, single-guide and three-guide plasmids (Fig. 2a and Supplementary Table 6) were packaged into AAV9 vectors by Vigene Biosciences. For intramuscular and temporal vein injection into neonatal pups, the dose of 7.5×10^{11} viral genomes each was used. Owing to the limitation in packaging capacity, two AAVs were needed for the three-guide cohort (Fig. 2a), therefore the total virus injected was 1.5×10^{12} viral genomes per mouse. Injection volume was brought to 50 μl with 1× PBS (Gibco). For treatment initiated at neonatal age, no randomization was performed, for example, the entire litter of P2 newborn pups were injected with either no-guide- or three-guide vectors.

For the tail vein injection in young, 3-week-old mice, 3 different doses were initially tested: 7.5×10^{10}, 1.5×10^{11} and 3×10^{11} viral genomes per gram of mouse (Extended Data Fig. 3). Randomization was performed among littermates. Similar to the intramuscular and temporal vein injections, two AAVs were needed for the three-guide cohort, therefore the total dose used in experiments described in Fig. 3 and Extended Data Figs. 4–10 was 6×10^{11} viral genomes per gram of mouse. Injection volume was brought to 100 μl with 1× PBS (Gibco). Detailed reporting of design, experimental procedures, mice and blinding are described in Supplementary Methods 1.

RNA isolation, guide screening and RT–PCR. RNA was isolated from cultured cells and mouse tissue sections, and cDNA synthesis was performed as previously described[3]. PCR amplification was used to assess the efficiency of each guide in upregulating *Lama1* expression using a primer in *Lama1* exon 55 (RDC 1919) and a second primer spanning the junction of exons 55 and 56 (RDC 1920). Sequences are listed in Supplementary Table 6.

qPCR using Fast SYBR green Master Mix (Qiagen) on a Step One Plus Real Time PCR (Applied Biosystems) was performed. *Lama1* expression was analysed using a primer in *Lama1* exon 55 (RDC 1919) and one spanning the junction of exons 55 and 56 (RDC 1920). Primers against endogenous *Gapdh* (RDC 345 and 346) were used as an internal control. $\Delta\Delta C_t$ was analysed to assess fold change in expression between treated and untreated samples.

Protein isolation and western blot. Proteins were isolated from dy^{2J}/dy^{2J} myoblasts and C2C12 cells by adding 150 μl of a 1:1 part solution of RIPA homogenizing buffer (50 mM Tris HCl pH 7.4, 150 nM NaCl, 1 mM EDTA) and RIPA double-detergent buffer (2% deoxycholate, 2% NP-40, 2% Triton X-100 in RIPA homogenizing buffer) supplemented with protease inhibitor cocktail (Roche). Proteins from mouse tissue sections were homogenized as previously described[3]. Total protein concentrations were measured using a Pierce BCA protein assay kit according to the manufacturer's protocol (Thermo Fisher Scientific). Western blots were performed as previously described[3]. Primary antibodies used were rabbit anti-LNα1 E3 (a gift from P. Yurchenco, 0.6 μg ml^{-1}), mouse monoclonal M2 anti-Flag (Sigma-Aldrich F1804, 1:1,000) and rabbit polyclonal anti-GAPDH (Santa Cruz sc-25778, 1:5,000). Uncropped gels are provided as Supplementary Fig. 1.

Immunofluorescence and haematoxylin and eosin staining. Muscles and nerves were sectioned at 8-μm thickness and processed for immunofluorescence analyses according to standard procedures. Antibodies used for immunofluorescence staining were rat monoclonal antibodies against laminin-α1 (mAb200, laboratory of M.D., 1:20), α2 (4H8-2, Sigma-Aldrich, 1:500), γ1 chain (clone A5, Thermo Fisher Scientific), a rabbit polyclonal antibody against laminin-α4 chain (provided by T. Sasaki), a mouse monoclonal antibody against NF-H (Biolegend SMI 31, 1:1,000), a goat polyclonal anti-rat Alexa Fluor 555 antibody (Thermo Fisher Scientific, 1:250) and a goat polyclonal anti-mouse Alexa Fluor 488 antibody (Thermo Fisher Scientific, 1:250). Haematoxylin and eosin staining was performed as previously described[2]. Both immunofluorescence and haematoxylin and eosin-stained slides were scanned with the 3Dhistech Pannoramic 250 Flash II digital scanner and analysed with CaseViewer software, with the exception of images shown in Extended Data Figs. 5, 6, which were analysed with a Zeiss Axioplan fluorescence microscope (Carl Zeiss) and images were captured using an ORCA 1394 ER digital camera (Hamamatsu Photonics) and Open Laboratory software version 4 (Improvision).

Toluidine blue staining and transmission electron microscopy. Freshly isolated mouse sciatic nerves were halved and fixed in a solution of 2% paraformaldehyde and 2.5% glutaraldehyde in 0.1 M sodium cacodylate buffer until further use. For embedding, the specimens were rinsed with the 0.1-M sodium cacodylate buffer, post-fixed in 1% osmium tetroxide in the washing buffer, dehydrated in a graded ethanol series followed by incubation in propylene oxide, and embedded in Quetol-Spurr resin overnight at 65 °C. Sections of 90-nm thickness were cut on a Leica EM UC7 ultramicrotome, stained with uranyl acetate and lead citrate, and imaged on a FEI Tecnai 20 electron microscope at 4,400×, 10,000× and 44,000× magnifications. The same 90-nm thick sections were stained with toluidine blue and imaged on a Leica DM-2000. All reagents were purchased from Electron Microscopy Sciences. Quantification of myelin thickness was measured using ImageJ from at least 14 random myelinated axons per field (at least 5 fields per mouse)[26]. No discrimination between axon diameters (for example, small or larger calibre nerves) was made during quantification.

Open field and in vivo muscle force assays. Open field activity test and assessment of in vivo muscle force were performed on tail-vein-injected cohorts at the Centre for Modelling Human Disease Mouse Phenotyping Facility of the Lunenfeld-Tanenbaum Research Institute. For the open field test, mice were placed in the frontal centre of a transparent Plexiglas open field (41.25 cm × 41.25 cm × 31.25 cm) illuminated by 200 lx. A trained operator, who was blinded to the nature of the projects and treatments, performed experiments. The VersaMax Animal Activity Monitoring System recorded vertical activities and total distance travelled for 20 min per mouse.

In vivo muscle contraction tests were performed using a 1300A: 3-in-1 Whole Animal System and analysed using the dynamic muscle control/analysis high-throughput software suite (Aurora Scientific). The mice were anaesthetized with intraperitoneal injection of a ketamine–xylazine cocktail at 100 mg kg^{-1} and 10 mg kg^{-1} of body weight, respectively. Contractile output was measured using percutaneous electrodes that stimulate specific nerves that innervate the plantar flexors. Specific tetanic force (200 ms of 0.5-ms pulses at 125 Hz) was recorded and corrected for body weight.

Nerve conduction velocity. Mice were anaesthetized with urethane (1.2 mg g^{-1}; intraperitoneal injection) and underwent a tracheotomy to maintain their airway but were not artificially ventilated. Core body temperature was maintained at 34–36.5 °C using a feedback-controlled heating pad (TR-200; Fine Science Tools). The sciatic nerve was exposed at two locations through incisions (around 15 mm) above the left knee (site 1) and along the sacral region of the vertebral column (site 2). After separating the nerve from adjacent tissue, a bipolar hook electrode was applied to the nerve at each site. Each electrode comprised two chloride silver wires (0.01-inch diameter, A-M systems) placed approximately 1 mm apart and bent at the tip to form hooks, and attached to a stimulator (Model DS3, Digitimer). Stimulating electrodes were insulated from the underlying tissue using a small piece of plastic paraffin film. Stimulus duration was fixed at 20 μs and the current intensity was varied. Stimulus timing was controlled by a computer using a Power1401 computer interface and Signal v.5 software (Cambridge Electronic Design). The compound muscle action potential (CMAP) was recorded using needle electrodes (~30G, BD PrecisionGlide), one inserted into the gastrocnemius muscle and the other (reference) electrode inserted into the Achilles tendon. The CMAP signal was amplified, low-pass-filtered at 10 Hz and high-pass-filtered at 1 kHz (DAM 80, World Precision Instruments), and digitized at 40 kHz using the Power1401 and Signal v.5 software (Cambridge Electronic Design). To calculate conduction velocity from CMAP responses, the sciatic nerve was stimulated at just-maximal intensity (beyond which there is no change in CMAP amplitude or latency) three times at site 1 and again three times at site 2. Nerve conduction velocity was calculated as the difference between mean CMAP latencies for each stimulation site divided by the length of nerve (7.5–10 mm) separating the sites.

Quantification of vector genomes. Evaluation of AAV genome distribution was performed as previously published[27] with a few modifications. Genomic DNA was extracted from tibialis anterior, sciatic nerve and liver of treated mice using

the Qiagen Blood and Tissue Kit. Then, 90 ng of DNA was amplified using primers located in between the two inverted tandem repeats (RDC 1687, RDC 1679; Supplementary Table 7) using Fast SYBR green master mix (Qiagen) on a Step One Plus Real Time PCR (Applied Biosystems). The C_t value of each reaction was converted to viral genome copy number by interpolating against the copy number of a standard curve of a known plasmid containing the sgRNA cassette (RDC 362). The amount of DNA input (90 ng per tissue) was used as a conversion factor to diploid genome (7 pg DNA = 1 diploid genome).

RNA-sequencing analyses. Total RNA was isolated from quadriceps muscles using the RNeasy kit (Qiagen) and quantified using a Qubit RNA HS assay (Thermo Fisher Scientific). RNA sequencing was performed by the Centre for Applied Genetics in Toronto using the Illumina HiSeq 2500 system, producing 120-bp paired-end reads. Alignment and analyses were performed as previously described[25]. In brief, raw transcript reads were aligned to the GRCm38 mouse genome (mm10) using HISAT2. HTSeq was used to determine the absolute number of read counts for each gene. Only genes with at least one read per million in at least three replicates were kept for downstream analysis. Normalization and differential expression analysis were completed using the R packages limma v.3.36.3 (https://bioconductor.org/packages/release/bioc/html/limma.html) and edgeR v.3.22.3 (https://bioconductor.org/packages/release/bioc/html/edgeR.html). Library sizes were scaled using trimmed mean of M-value normalization applied using the edgeR package. Using limma, paired sample data were fitted to a linear model, then all pairwise comparisons were made. False discovery and multiple testing were controlled for and an adjusted P value was computed using the Benjamini–Hochberg method. Differentially expressed genes were defined as genes with a more than twofold change and adjusted $P < 0.05$. Off-target analysis was conducted using a list of 704 computationally predicted using Cas-OFFinder. Using the Bedtools suite 'closest' function, each of the top 100 differentially expressed genes was matched to the nearest off-target loci to determine the shortest distance from off-target loci to differentially expressed gene body.

Statistical analyses. Statistical analyses for every experiment are described accordingly in the figure legends. Unless specified, GraphPad Prism version 8 was used to perform most statistical analyses.

Reporting summary. Further information on research design is available in the Nature Research Reporting Summary linked to this paper.

Data availability

The authors declare that the main data supporting the findings of this study are available within the paper and its Supplementary Information.

26. Zhang, Y. et al. Notch1 signaling plays a role in regulating precursor differentiation during CNS remyelination. *Proc. Natl Acad. Sci. USA* **106**, 19162–19167 (2009).
27. Hakim, C. H. et al. A five-repeat micro-dystrophin gene ameliorated dystrophic phenotype in the severe DBA/2J-mdx model of Duchenne muscular dystrophy. *Mol. Ther. Methods Clin. Dev.* **6**, 216–230 (2017).

a

b

c

d
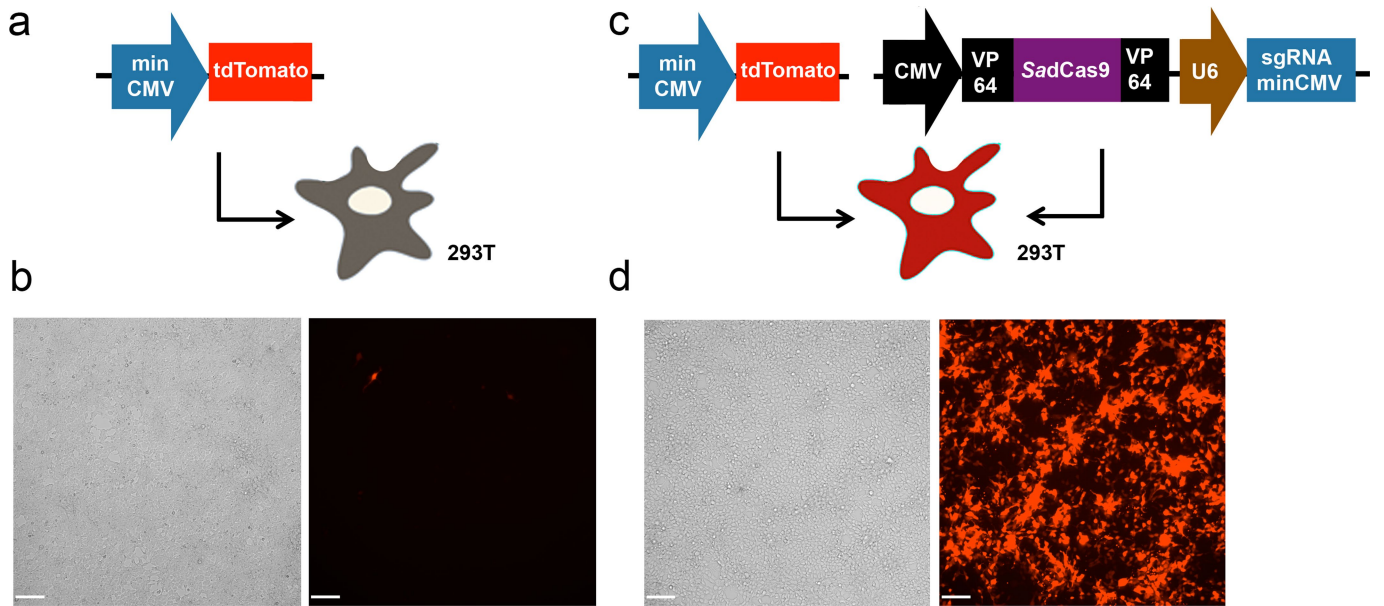
Extended Data Fig. 1 | SadCas9–2×VP64 enhances expression of minCMV-driven tdTomato in vitro. a, **b**, HEK293T cells were transfected with a plasmid encoding minCMV-driven tdTomato only. **c**, **d**, HEK293T cells were transfected with a combination of a plasmid containing minCMV-driven tdTomato and one containing SadCas9–2×VP64 and a sgRNA targeting the minCMV promoter. **a**, **c**, Schematic. **b**, **d**, Cells were imaged for tdTomato expression by fluorescent microscopy. Bright-field and tdTomato images are shown. The experiment was repeated three times independently with similar results. Scale bars, 50 μm.
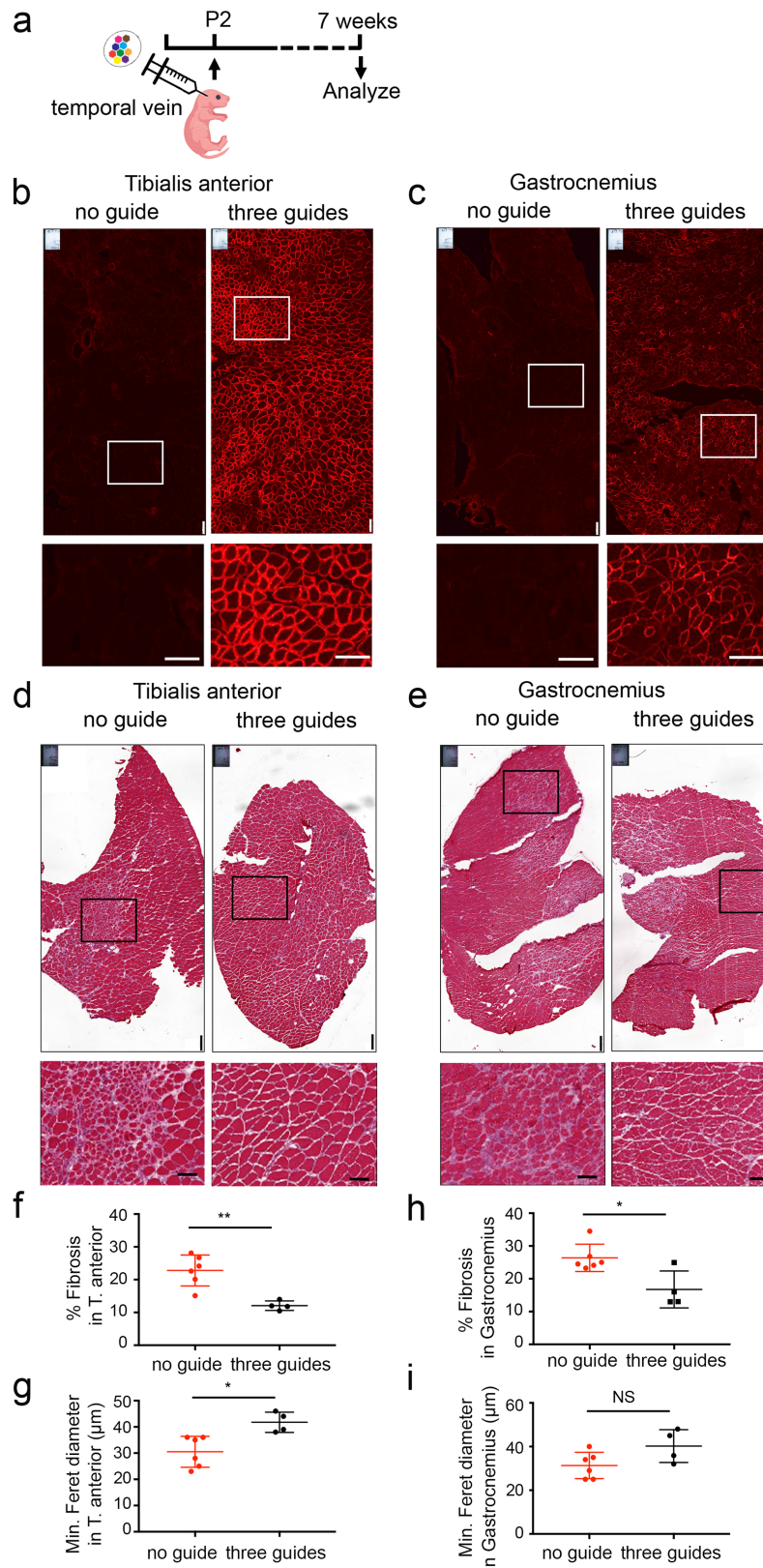
Extended Data Fig. 2 | Early intervention to upregulate Lama1 prevents disease progression in dy^{2j}/dy^{2j} mice. a, P2 neonatal dy^{2j}/dy^{2j} mice were injected with AAV9s carrying no guide ($n = 6$; 7.5×10^{11} viral genomes) or three guides ($n = 4$; split into two vectors; total dose of $2 \times 7.5 \times 10^{11}$ viral genomes) in the temporal vein and euthanized 7 weeks later. **b, c**, Immunofluorescence staining shows Lama1 expression in tibialis anterior (**b**) and gastrocnemius (**c**) muscles. Scale bars, 100 μm. **d, e**, General muscle histopathology was evaluated by haematoxylin and eosin staining on tibialis anterior (**d**) and gastrocnemius (**e**) muscles.

Scale bars, 200 μm. All mice ($n = 6$, no guide and $n = 4$, three guides) were analysed for experiments shown in **b**–**e**, which were repeated three times independently with similar results. **f**–**i**, Fibrosis (**f, h**) and minimum Feret diameter (**g, i**) were quantified for all mice from both treatment groups ($n = 6$, no guide and $n = 4$, three guides) by two independent experimenters with similar results. Data are mean ± s.d. **$P = 0.0025$ (**f**), *$P = 0.0103$ (**g**), *$P = 0.0142$ (**h**), $P = 0.0711$ (**i**); two-tailed Student's t-test.
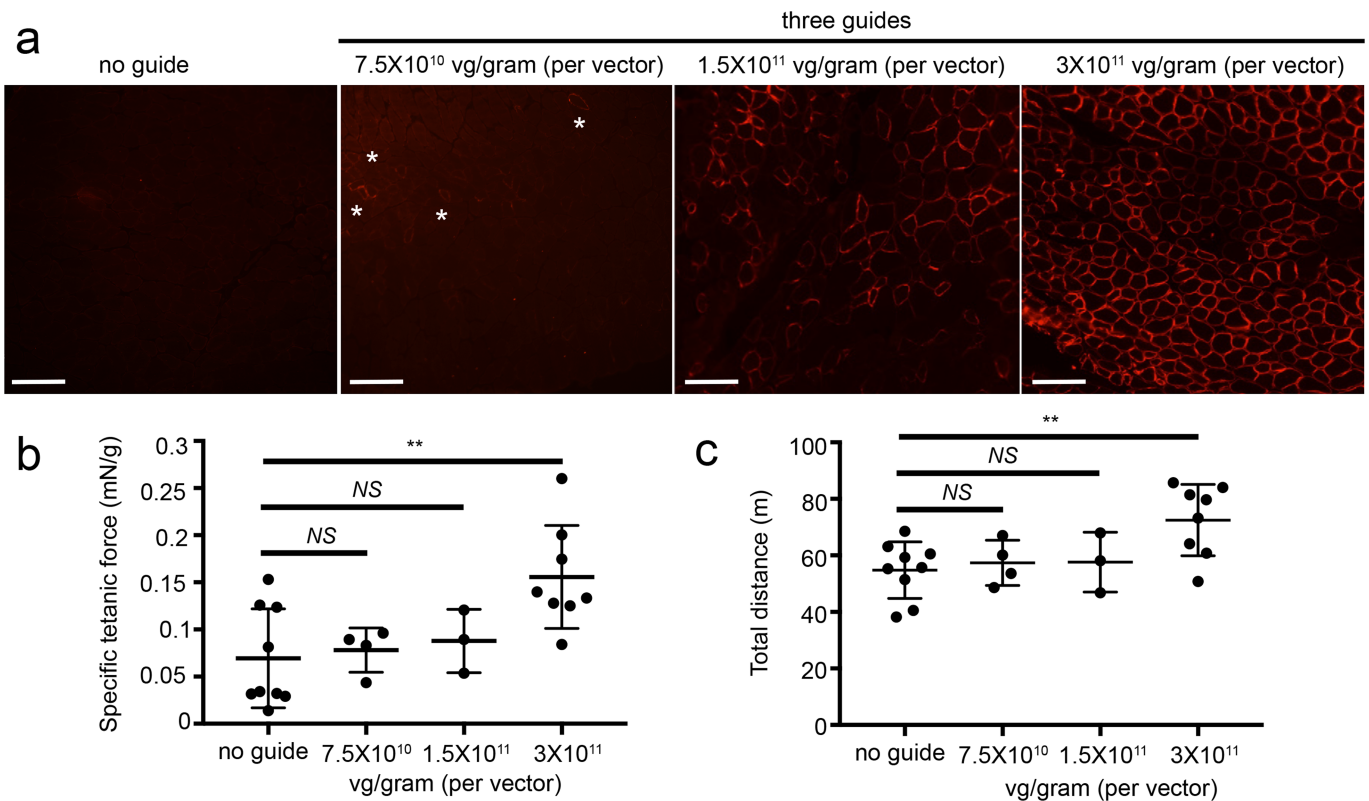
Extended Data Fig. 3 | Upregulation of Lama1 corresponds to improvement of muscle functions. Three-week-old dy^{2j}/dy^{2j} mice were injected systemically in the tail vein with AAV9s carrying no guide ($n = 9$) at the dose of 3×10^{11} viral genomes (vg) per gram of mouse, or three guides at different doses of 7.5×10^{10} ($n = 4$), 1.5×10^{11} ($n = 3$) or 3×10^{11} ($n = 8$) viral genome per gram of mouse. Two AAVs were needed for the three-guide cohorts, therefore the total doses of virus injected were 1.5×10^{11}, 3×10^{11} and 6×10^{11} viral genomes per gram of mouse. **a**, Tibialis anterior muscles isolated that were isolated four weeks later were stained for Lama1 expression. Asterisks indicate Lama1-positive fibres in the low-dose cohort. The experiment was repeated three times independently with similar results. Scale bars, 100 μm. **b**, **c**, In vivo contractile force assays (**b**) and open field tests (**c**) were performed at the end of the treatment regimen. Data are mean ± s.d. **b**, P values from left to right are: $P = 0.9849$, $P = 0.9082$, **$P = 0.0044$; one-way ANOVA with Dunnett's multiple comparisons test. **c**, P values from left to right are: $P = 0.9640$, $P = 0.9646$, **$P = 0.0085$; one-way ANOVA with Dunnett's multiple comparisons test.
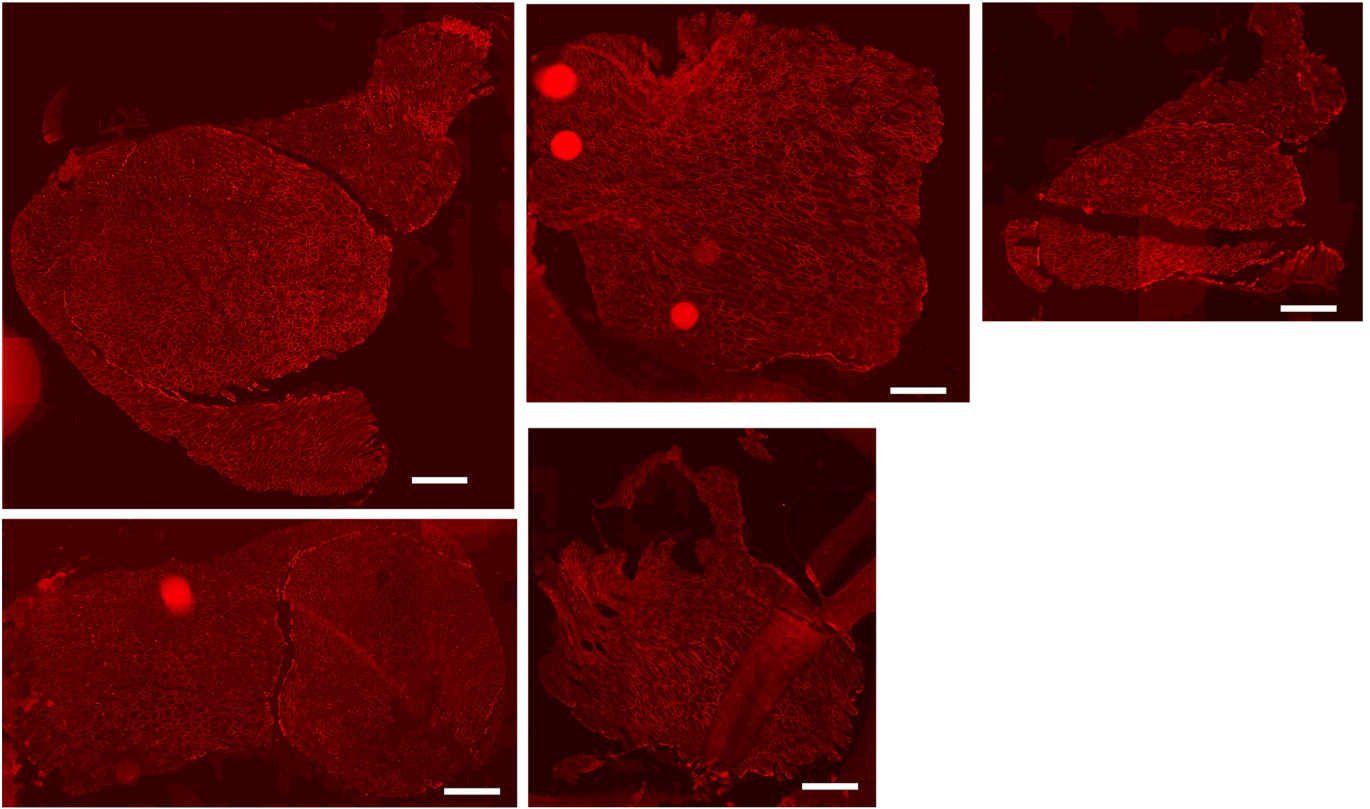
Extended Data Fig. 4 | Representative images of Lama1-positive muscle sections. Three-week-old mice were injected systemically with three guides ($n = 5$) at the dose of 3×10^{11} viral genomes per gram of mouse (split into two vectors, thus total dose was $2 \times 3 \times 10^{11}$ viral genomes per gram of mouse) in the tail vein, and euthanized at the age of 11–12 weeks old. Muscles were stained for Lama1 expression (red). Scale bars, 500 μm. The experiment was repeated three times independently with similar results.
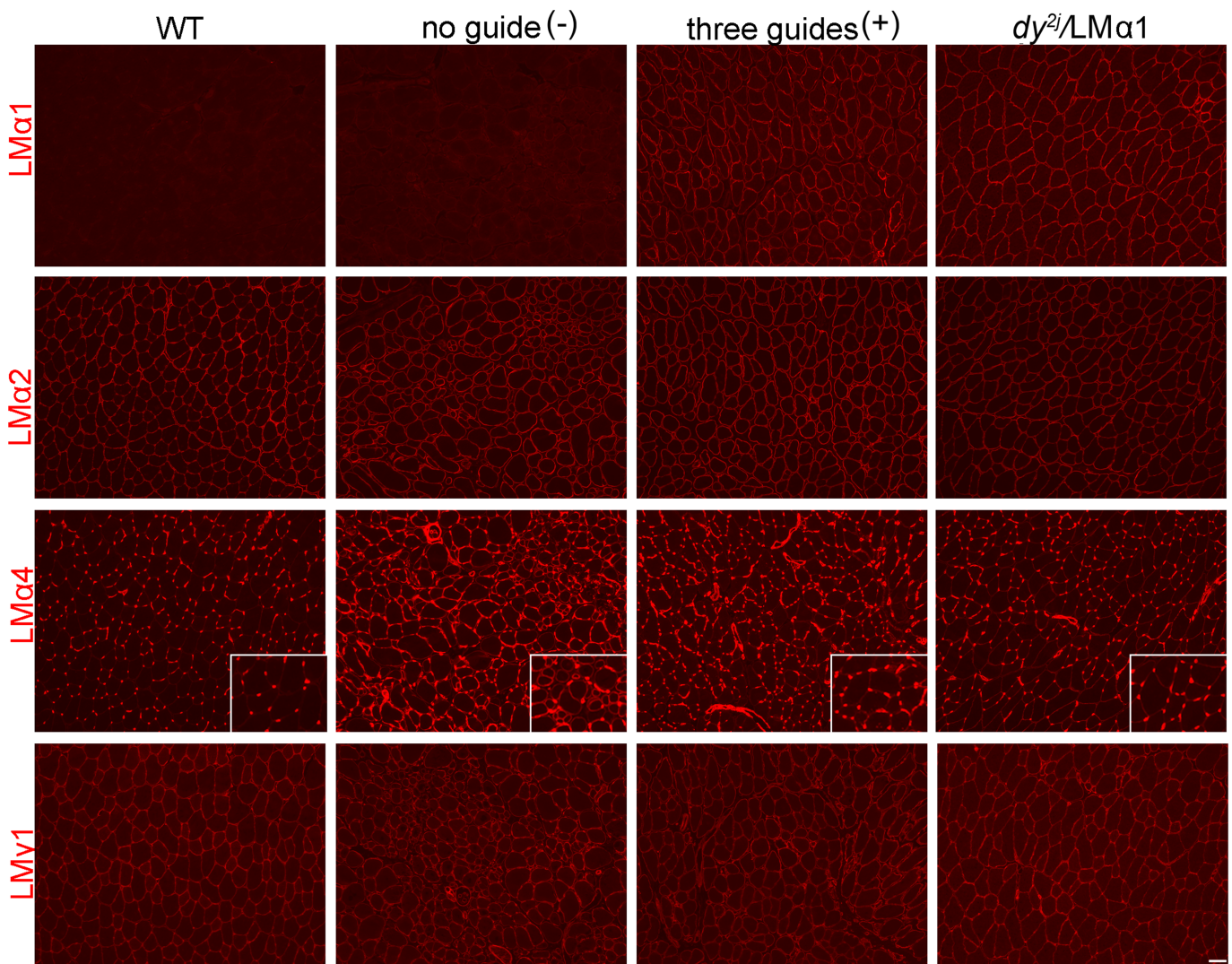
Extended Data Fig. 5 | Expression of laminin subunits in tibialis anterior muscles. Expression of laminin (LM) subunits in tibialis anterior muscles of wild-type, dy^{2j}/dy^{2j} (intravenously injected with AAVs carrying no guide at 3×10^{11} viral genomes per gram of mouse or three guides at a total dose of $2 \times 3 \times 10^{11}$ viral genomes per gram of mouse) and dy^{2j}/dy^{2j} LMα1 (with transgenic overexpression of LMα1) mice ($n = 3$ for each group). Expression of the LMα1 chain in the tibialis anterior muscle is comparable between dy^{2j}/dy^{2j} mice treated with three guides and transgenic mice. No major differences in expression of LMα2 and LMγ1 were detected between the groups. The LMα4 chain is upregulated in muscles of dy^{2j}/dy^{2j} mice treated with the no-guide AAV and the expression of the LMα4 chain is partially normalized in muscle of dy^{2j}/dy^{2j} mice treated with the three-guide AAV. Scale bar, 50 μm. The experiment was repeated three times independently with similar results.
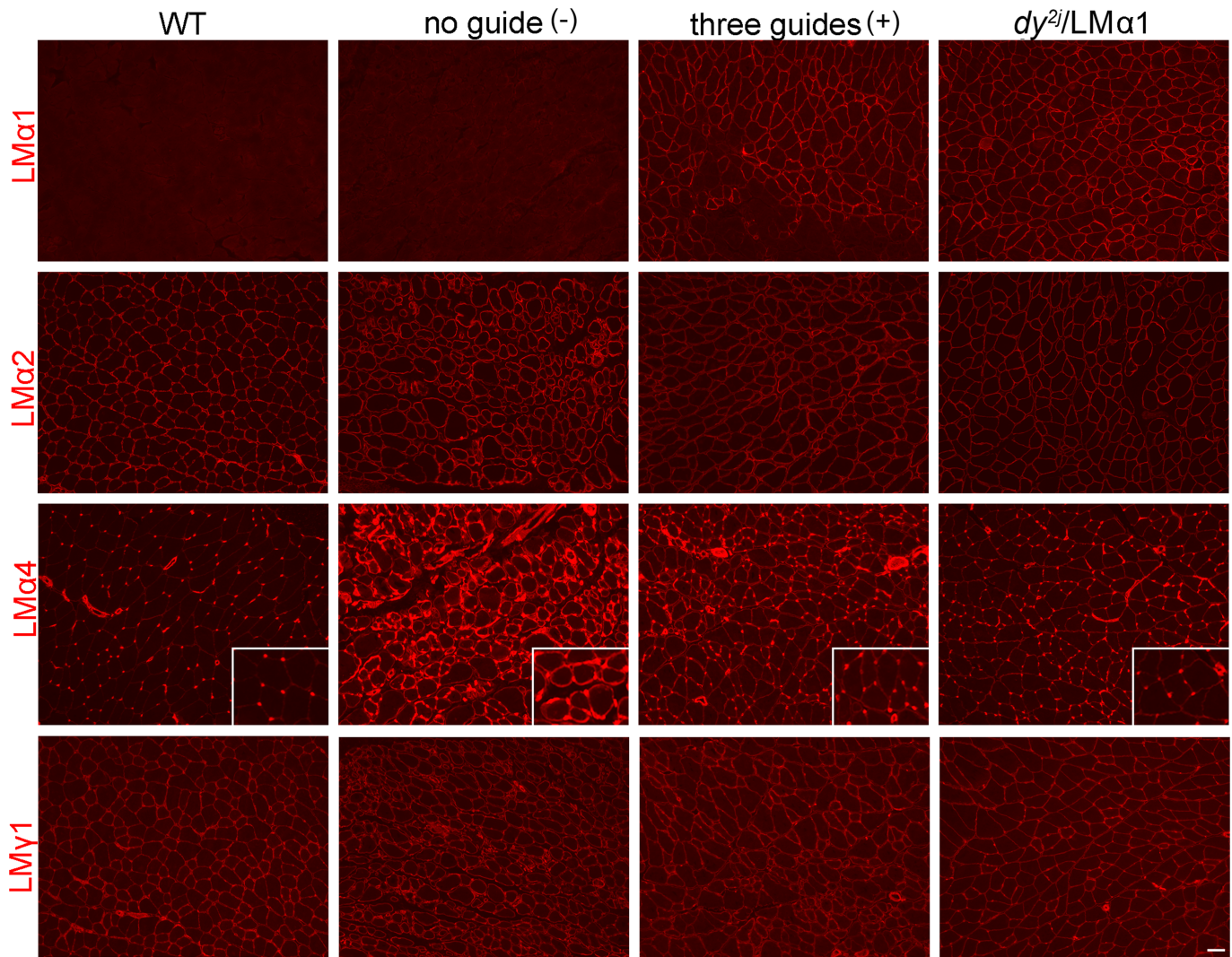
Extended Data Fig. 6 | Expression of laminin subunits in gastrocnemius muscles. Expression of laminin subunits in gastrocnemius muscles from wild-type, dy^{2j}/dy^{2j} (intravenously injected with AAVs carrying no guide at 3×10^{11} viral genomes per gram of mouse or three guides at a total dose of $2 \times 3 \times 10^{11}$ viral genomes per gram of mouse) and dy^{2j}/dy^{2j} LMα1 (with transgenic overexpression of LMα1) mice ($n = 3$ for each group). Expression of the LMα1 chain in the gastrocnemius muscles is comparable between dy^{2j}/dy^{2j} mice treated with three guides and transgenic mice. No major differences in expression of LMα2 and LMγ1 were detected between the groups. The LMα4 chain is upregulated in muscle of dy^{2j}/dy^{2j} mice treated with the no-guide AAV and the expression of the LMα4 chain is partially normalized in muscle of dy^{2j}/dy^{2j} AAV-mice treated with three guides. Scale bar, 50 μm. The experiment was repeated three times independently with similar results.
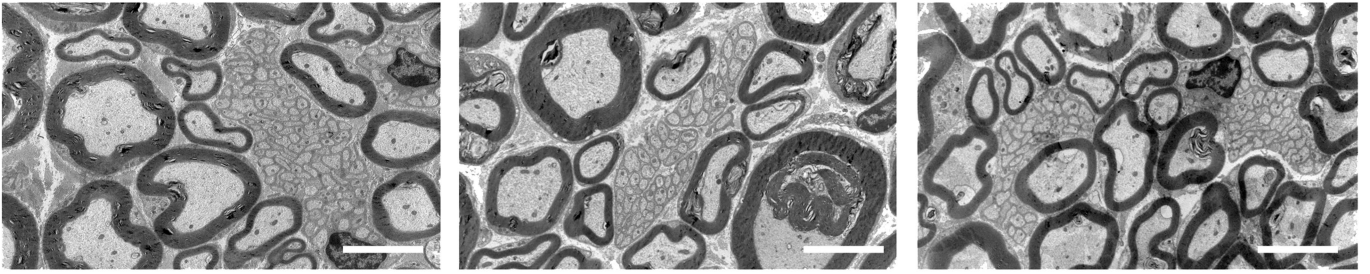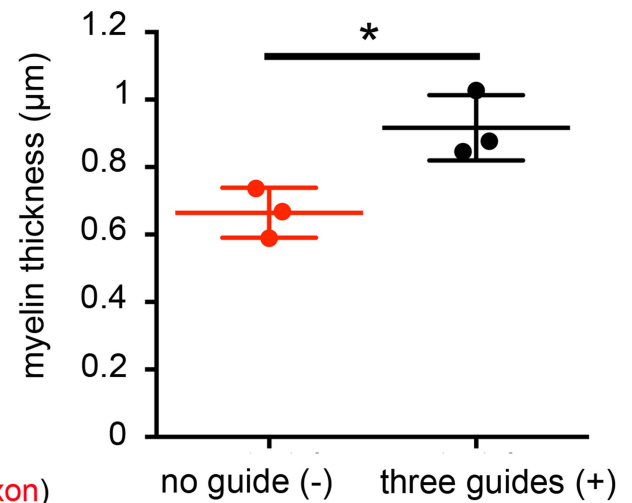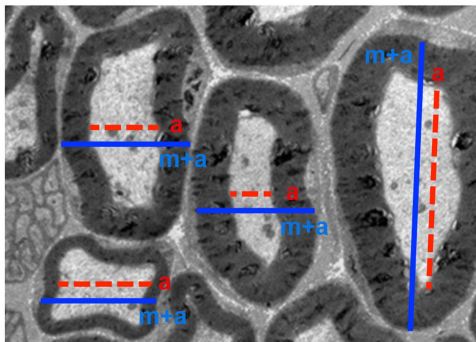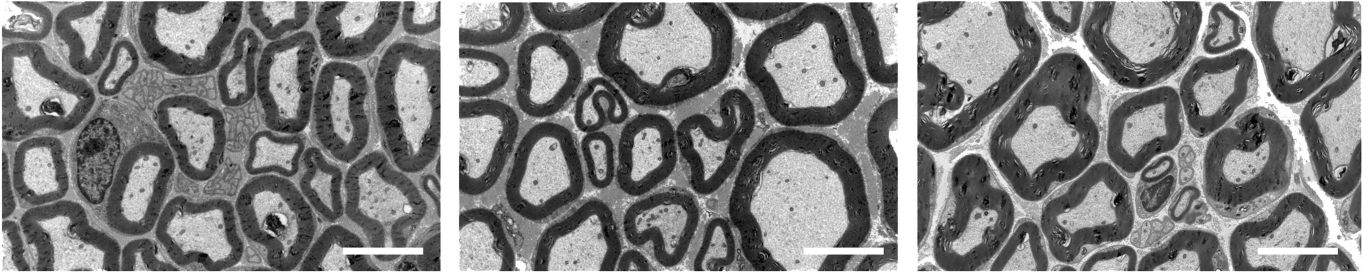
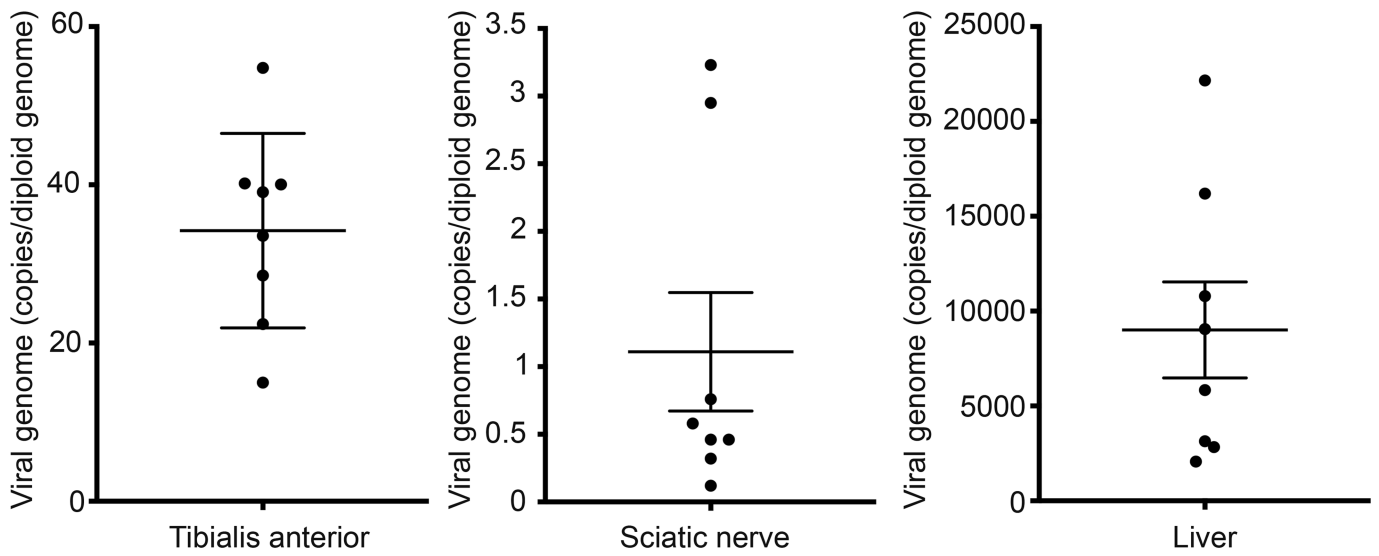**Extended Data Fig. 7 | Myelination of sciatic nerves.** Transmission electron microscopy images of sciatic nerves isolated from dy^{2j}/dy^{2j} mice injected with AAV9s carrying no guide (3×10^{11} viral genomes per gram of mouse) or three guides (split into two vectors; total dose of $2 \times 3 \times 10^{11}$ viral genomes per gram of mouse). Three mice were analysed per group. Myelin thickness was measured as the difference between the distance of the myelin and axon (m+a, blue solid line) and axon only (a; red dotted line), quantified using ImageJ and presented as mean $\pm$ s.d. Statistical analysis was performed using a two-tailed t-test. $*P = 0.0231$. Scale bar, 5 µm. The experiment was repeated three times independently with similar results.

Extended Data Fig. 8 | Quantitative evaluation of AAV genome distribution. Genomic DNA isolated from the tibialis anterior muscle, sciatic nerve and liver of dy^{2j}/dy^{2j} mice ($n = 8$) injected with AAVs carrying three guides at the dose of 3×10^{11} viral genomes per gram of mouse (split into two vectors; total dose of $2 \times 3 \times 10^{11}$ viral genomes per gram of mouse) was amplified to analyse the presence of viral genomes by qPCR. Data are mean ± s.e.m. The experiment was repeated three times independently with similar results.
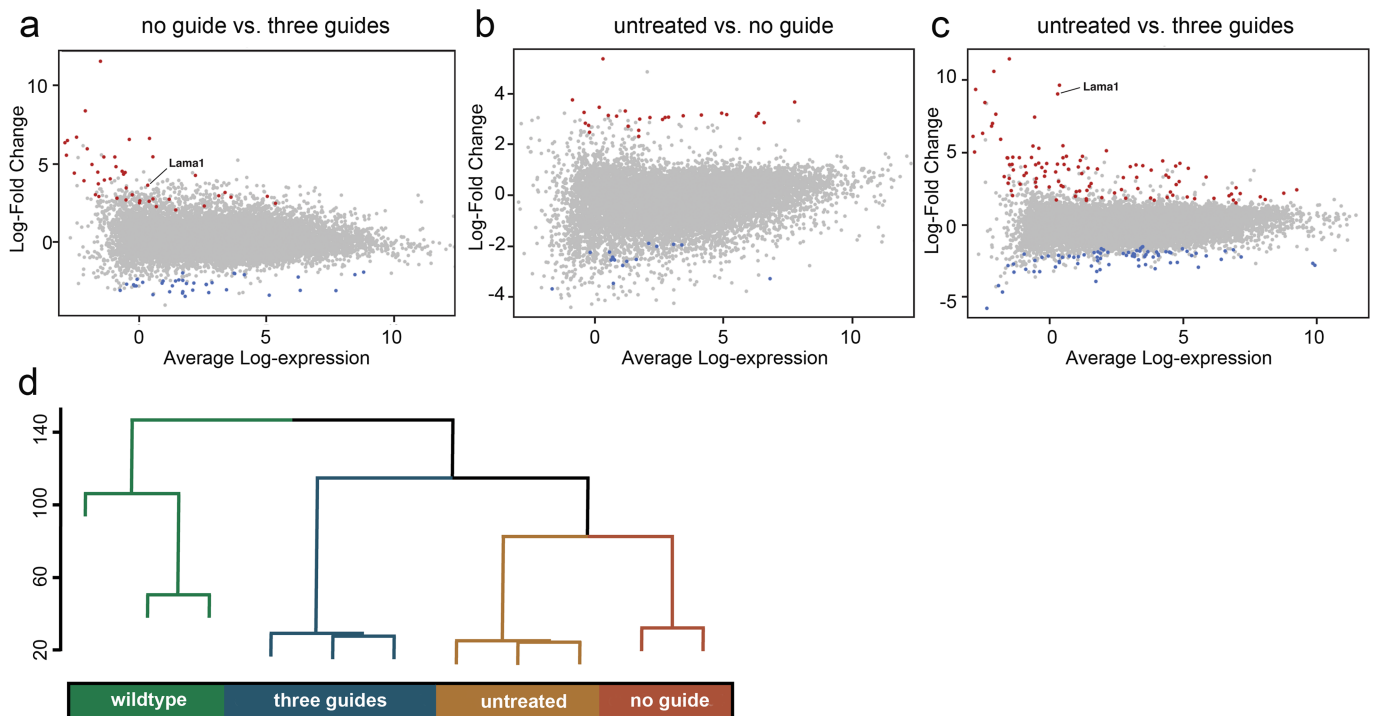
Extended Data Fig. 9 | Genome-wide analysis of gene expression of **SadCas9-2×VP64-treated** dy^{2j}/dy^{2j} **mice. a–c,** Differential expression analysis derived from RNA-sequencing results from the quadriceps of treated and untreated mice ($n = 3$ per group). **a, b,** No guide: dy^{2j}/dy^{2j} mice injected with AAV9 carrying only the SadCas9–2×VP64 at the dose of 3×10^{11} viral genomes per gram of mouse. **a, c,** Three guides: dy^{2j}/dy^{2j} mice injected with AAV9 carrying the SadCas9–2×VP64 and three guides at the dose of 3×10^{11} viral genomes per gram of mouse (total dose of $2 \times 3 \times 10^{11}$ viral genomes per gram of mouse). **b, c,** Untreated: dy^{2j}/dy^{2j} mice that had not been injected with AAV9. False discovery and multiple testing were controlled for and an adjusted P value was computed using the Benjamini–Hochberg method. Differentially expressed genes were defined as genes with a more than twofold change and adjusted $P < 0.05$. For each comparison, significantly differentially expressed genes (false-discovery rate-adjusted $P < 0.05$) are coloured. Red data points indicate a log-transformed fold change in expression greater than one; blue data points indicate a log-transformed fold change in expression less than one. **d,** Hierarchical clustering was performed on the normalized counts-per-million expression data.
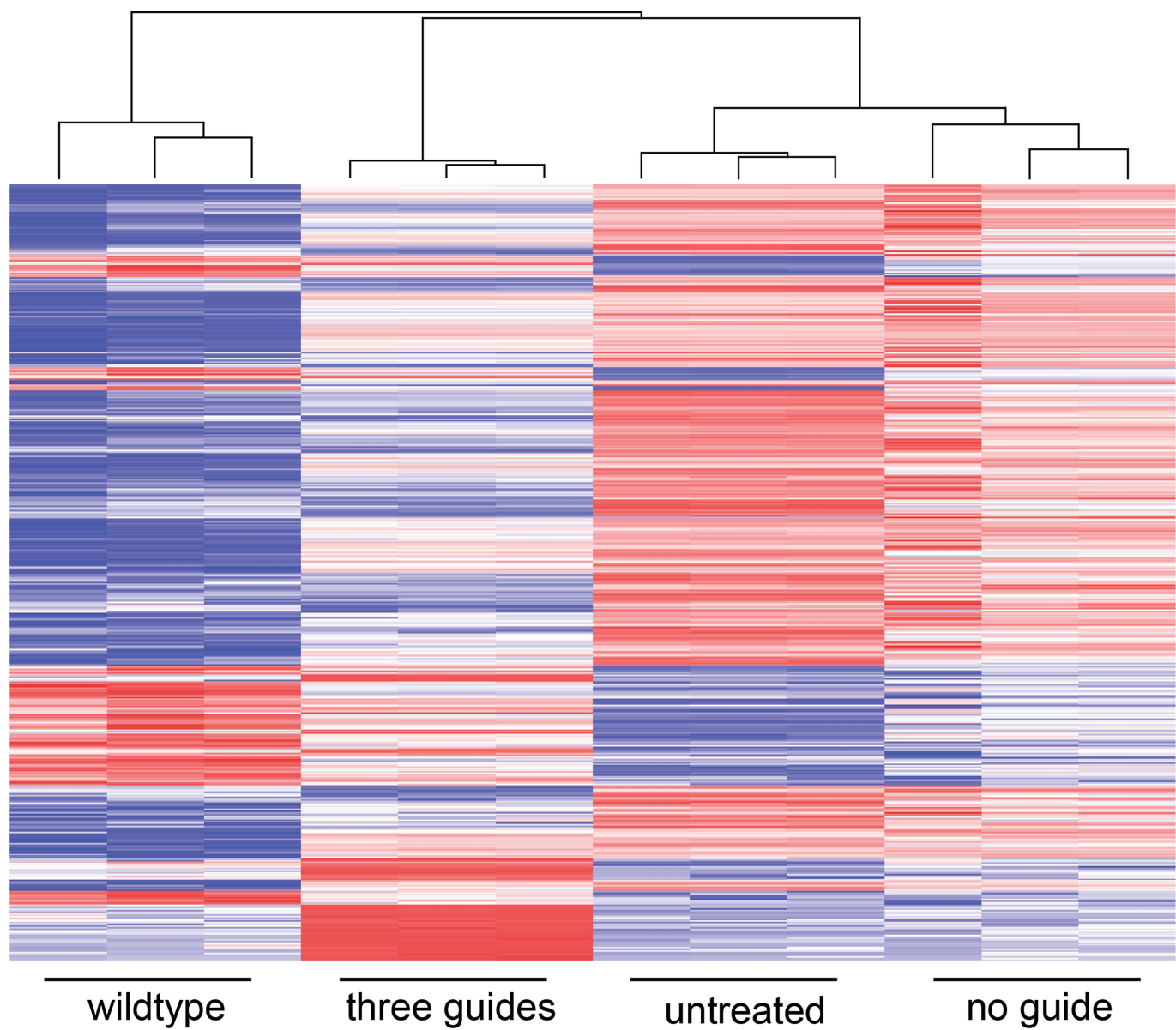
Extended Data Fig. 10 | Top 500 differentially expressed genes.
Heat map illustrating the log-normalized counts per million for the top 500 genes that were differentially expressed in quadriceps isolated from wild-type mice, or dy^{2j}/dy^{2j} mice injected with AAV9s carrying SadCas9–2×VP64 only (no guide, $n = 3$) or with three guides (three guides, $n = 3$), and compared to age-matched, untreated dy^{2j}/dy^{2j} mice. Red indicates higher expression; blue indicates lower expression.

Corresponding author(s):   Ronald D. Cohn

Reporting Summary

Nature Research wishes to improve the reproducibility of the work that we publish. This form provides structure for consistency and transparency in reporting. For further information on Nature Research policies, see Authors & Referees and the Editorial Policy Checklist.

Statistical parameters

When statistical analyses are reported, confirm that the following items are present in the relevant location (e.g. figure legend, table legend, main text, or Methods section).

n/a	Confirmed	
☐	☒	The exact sample size (*n*) for each experimental group/condition, given as a discrete number and unit of measurement
☐	☒	An indication of whether measurements were taken from distinct samples or whether the same sample was measured repeatedly
☐	☒	The statistical test(s) used AND whether they are one- or two-sided *Only common tests should be described solely by name; describe more complex techniques in the Methods section.*
☒	☐	A description of all covariates tested
☒	☐	A description of any assumptions or corrections, such as tests of normality and adjustment for multiple comparisons
☒	☐	A full description of the statistics including central tendency (e.g. means) or other basic estimates (e.g. regression coefficient) AND variation (e.g. standard deviation) or associated estimates of uncertainty (e.g. confidence intervals)
☐	☒	For null hypothesis testing, the test statistic (e.g. *F*, *t*, *r*) with confidence intervals, effect sizes, degrees of freedom and *P* value noted *Give P values as exact values whenever suitable.*
☒	☐	For Bayesian analysis, information on the choice of priors and Markov chain Monte Carlo settings
☒	☐	For hierarchical and complex designs, identification of the appropriate level for tests and full reporting of outcomes
☒	☐	Estimates of effect sizes (e.g. Cohen's *d*, Pearson's *r*), indicating how they were calculated
☐	☒	Clearly defined error bars *State explicitly what error bars represent (e.g. SD, SE, CI)*

Our web collection on statistics for biologists may be useful.

Software and code

Policy information about availability of computer code

Data collection	For RNA-Seq: R packages limma, v3.36.3 and edgeR, v.3.22.3.
Data analysis	For RNA-Seq: R packages limma, v3.36.3 and edgeR, v.3.22.3.

For manuscripts utilizing custom algorithms or software that are central to the research but not yet described in published literature, software must be made available to editors/reviewers upon request. We strongly encourage code deposition in a community repository (e.g. GitHub). See the Nature Research guidelines for submitting code & software for further information.

Data

Policy information about availability of data

All manuscripts must include a data availability statement. This statement should provide the following information, where applicable:
- Accession codes, unique identifiers, or web links for publicly available datasets
- A list of figures that have associated raw data
- A description of any restrictions on data availability

The authors declare that the data supporting the findings of this study are available within the paper and its supplementary information files.

Field-specific reporting

Please select the best fit for your research. If you are not sure, read the appropriate sections before making your selection.

☒ Life sciences ☐ Behavioural & social sciences ☐ Ecological, evolutionary & environmental sciences

For a reference copy of the document with all sections, see nature.com/authors/policies/ReportingSummary-flat.pdf

Life sciences study design

All studies must disclose on these points even when the disclosure is negative.

Sample size	No sample-size calculation was performed. Number of animals were similar to our previous study (PMID: 28714989) and as recommended by TREAT-NMD SOP, which range from 3-9 animals per treatment group.
Data exclusions	No data were excluded from analyses.
Replication	For in vitro experiments, three independent biological experiments were performed (Fig 1 legend). For in vivo experiments (Figs 2-3, Extended Fig. 2-8), number of animals per group are treated as biological replicates.
Randomization	For treatment started at 3-weeks old (Figs. 2 and 3), randomization was performed among littermates. For treatment initiated at neonatal P2 (Extended Fig. 2), no randomization was performed, e.g. the entire litter of P2 newborns were injected with either "no guide" or "three guides" vectors.
Blinding	A trained operator who is unaware of the nature of the projects and treatments performed functional tests. Investigators who performed morphometric analyses, e.g. fibrosis, fiber size and myelin thickness were blinded as well.

Reporting for specific materials, systems and methods

Materials & experimental systems

n/a	Involved in the study
☒	☐ Unique biological materials
☐	☒ Antibodies
☐	☒ Eukaryotic cell lines
☒	☐ Palaeontology
☐	☒ Animals and other organisms
☒	☐ Human research participants

Methods

n/a	Involved in the study
☒	☐ ChIP-seq
☒	☐ Flow cytometry
☒	☐ MRI-based neuroimaging

Antibodies

Antibodies used	Information for anti-LNalpha1 E3 (rabbit), -FLAG M2, -GAPDH, -LNalpha1 (rat), -LNalpha2 (rat), -LNgamma1 (rat), -LNalpha4 (rabbit), -NF-H (mouse), Alexa Fluor 555 (rat), Alexa Fluor 488 (mouse) are provided in Methods section.
Validation	Anti-LNalpha1 E3 (rabbit) for Western blot and -LNalpha1 (rat) -LNalpha2 (rat), -LNgamma1 (rat), -LNalpha4 (rabbit) for IF staining were validated on transgenic mouse model overexpressing Laminin-alpha-1 generated in Dr. Durbeej's laboratory. FLAG M2 was optimized for single banded detection of FLAG fusion proteins in mammalian system (Sigma Aldrich website). GAPDH was validated on 293T and A549 whole cell lysates (Santa Cruz website). NF-H was validated on SH-SY5Y neuroblastoma and rat brain tissue (Biolegend website). Secondary Alexa Fluor 555 and 488 were validated based on standard company's quality control procedure (Thermo website).

Eukaryotic cell lines

Policy information about cell lines

Cell line source(s)	HEK 293 and C2C12 were obtained from ATCC
Authentication	None of the cell lines used were authenticated.
Mycoplasma contamination	All cell lines were tested negative for mycoplasma.

Commonly misidentified lines (See ICLAC register)	N/A

Animals and other organisms

Laboratory animals	The dy2j/dy2j and C57BL/6J mice used for experiments were 2 days- or 3 weeks old. Both males and females were used.
Wild animals	The study did not involve wild animals.
Field-collected samples	The study did not involve samples collected from the field.